Geometry of the Feasible Output Regions of Grid-Interfacing Inverters with Current Limits

Lauren Streitmatter, Trager Joswig-Jones and Baosen Zhang

Abstract—Many resources in the grid connect to power grids via programmable grid-interfacing inverters that can provide grid services and offer greater control flexibility and faster response times compared to synchronous generators. However, the current through the inverter needs to be limited to protect the semiconductor components. Existing controllers are designed using somewhat ad hoc methods, for example, by adding current limiters to preexisting control loops, which can lead to stability issues or overly conservative operations.

In this paper, we study the geometry of the feasible output region of a current-limited inverter. We show that under a commonly used model, the feasible region is convex. We provide an explicit characterization of this region, which allows us to efficiently find the optimal operating points of the inverter. We demonstrate how knowing the feasible set and its convexity allows us to design safe controllers such that the transient trajectories always remain within the current magnitude limit, whereas standard droop controllers can lead to violations.

Index Terms—Power systems, Optimization, Energy systems

I. Introduction

Many resources in the electric system, including solar PV, wind, storage, and electric vehicles (EVs), are connected to the grid through power electronic inverters. At the same time, power systems were designed assuming the presence of large spinning machines [1]. As fossil fuel-based generation retires and inverter-based resources (IBRs) grow, understanding whether the latter could successfully replace the former in grid operations is becoming increasingly important.

A key difference between IBRs and synchronous generators is their ability to handle current during normal and contingent operations [2], [3]. Synchronous generators can typically supply more than 5 to 10 times their rated current with relatively little damage [4]. In contrast, in order to protect semiconductor devices, inverter currents can only marginally exceed their nominal rated currents [5], [6]. In recent years, significant attention has been paid to how currents should be limited, for example, see [2], [3], [7], [8] and the references within.

However, despite these results, the dispatch signals coming from the system are often somewhat oblivious to the current limits. In most cases, inverters are expected to track some setpoints, for example, current/power for grid following inverters and voltage/power for grid forming inverters [9]–[11]. These setpoints are optimized to maximize the efficiency of the overall system, but they may not include the physical constraint of the inverters. Even when the inverter constraints are included, they are often presented in simple forms (e.g.

Department of Electrical and Computer Engineering, University of Washington Seattle, WA 98195, USA {lstreit, joswitra, zhangbao}@uw.edu

The authors are partially supported by the NSF grant ECCS-1942326, the Washington Clean Energy Institute, the Grainger Foundation and the Galloway Foundation.

upper and lower bounds on all quantities) which do not match the geometry of the actual feasible operation regions.

Inverters achieve given setpoints using control loops (typically a current loop and a voltage loop). But if reaching these setpoints leads to a violation of the current rating, the inverter output current would saturate [3], resulting in a mismatch between the higher-level commands and the physical limit of the device. Depending on how the current limiter is designed, the inverter could become dynamically unstable and could cause severe problems in a grid [12]–[15].

In this paper, we study the geometry of the feasible operating region of a current-limited inverter. That is, given a current limit and the inverter parameters, what is the region of all achievable outputs? Answering this question is the natural first step towards ensuring the safe operations of inverters and designing controllers that optimize their performances. We show that, under a commonly used model, the feasible region is convex when two of active power, reactive power and square of the voltage magnitudes ¹ are considered. We provide an explicit characterization of this region using linear matrix inequalities, so we can efficiently find the optimal operating points of the inverter.

Because power and voltage magnitude depend quadratically on the current, and the current is a vector in \mathbb{R}^2 (in the dq frame), the feasible region is a quadratic map of a disk (current magnitude is upper bounded). Unlike affine transformations, a quadratic map of a convex set is not, in general, convex. It turns out that the particular structure of the inverter circuit preserves convexity, which we will explain in detail in this paper. We also demonstrate how knowing the feasible set and its convexity allows us to design safe controllers such that the transient trajectories always remain within the current magnitude limit, whereas standard droop controllers can lead to violations.

II. MODEL AND PROBLEM FORMULATION

A. Inverter Model

In this study, we consider a widely used model of a three-phase inverter connected to an infinite bus through an RL branch as shown in Figure 1 [14], [16]. The model assumes a balanced three-phase system and can thus use the direct-quadrature (dq) frame transformation with reference to some angle θ rotating at constant frequency ω to describe all the rotating physical quantities in \mathbb{R}^2 rather than \mathbb{R}^3 . We assume the grid-side voltage is of constant magnitude, E, and define \mathbf{E}_{dq} with respect to the grid-side voltage angle, θ , to get $\mathbf{E}_{\mathrm{dq}} = (E,0)$. The dynamics of a voltage-source inverter

¹It is more common to consider the magnitude of voltage and not its square. However, the squared magnitude is much easier to work with.

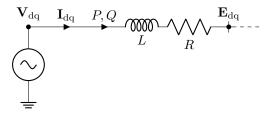


Fig. 1. We model the inverter as a controllable voltage source in the ${\rm dq}$ -frame connected via an RL filter to an infinite bus.

connected to \mathbf{E}_{dq} through resistor R and inductor L are governed by

$$\begin{bmatrix} \dot{I}_{\rm d} \\ \dot{I}_{\rm q} \end{bmatrix} = \mathbf{A} \begin{bmatrix} I_{\rm d} \\ I_{\rm q} \end{bmatrix} + \frac{1}{L} \begin{bmatrix} V_{\rm d} - E \\ V_{\rm q} \end{bmatrix}, \tag{1}$$

where $\mathbf{A} = \begin{bmatrix} -R/L & \omega \\ -\omega & -R/L \end{bmatrix}$, and \mathbf{I}_{dq} and \mathbf{V}_{dq} are the inverter current and voltage, respectively, in the dq-reference frame of the grid [16]. We will treat \mathbf{I}_{dq} as the state and \mathbf{V}_{dq} as the control input. We note that \mathbf{A} is skew-symmetric with equal diagonal elements. This is the key structural property of the inverter that allows us to derive the main results.

To protect the semiconductor switches, the magnitude of the current should be limited [17], [18]. We denote this limit as $I_{\rm max}$ and we define the safe (or feasible) current operating region as

$$\mathcal{I} := \{ \mathbf{I}_{dq} \mid \|\mathbf{I}_{dq}\|_2^2 \le I_{max}^2 \}.$$

B. Inverter Output

Inverters in the grid are usually asked to optimize their output, typically a combination of active power, reactive power, and voltage magnitude. The natural question becomes how well we can optimize these outputs given the constraint that current needs to stay in the safe region \mathcal{I} .

The inverter's active power, reactive power, and the squared voltage magnitude are all expressed as quadratic functions of the current and the voltage:

$$P = \frac{3}{2} \mathbf{I}_{\mathrm{dq}}^T \mathbf{V}_{\mathrm{dq}} \tag{2a}$$

$$Q = \frac{3}{2} \mathbf{I}_{\mathrm{dq}}^T \mathbf{J} \mathbf{V}_{\mathrm{dq}}$$
 (2b)

$$V_{\rm dq}^2 = \mathbf{V}_{\rm dq}^T \mathbf{V}_{\rm dq}, \tag{2c}$$

where $\mathbf{J} = \begin{bmatrix} 0 & 1 \\ -1 & 0 \end{bmatrix}$. We note that it is more common to consider the voltage magnitude rather than the squared magnitude as we do here. Of course, the two are equivalent from the point of view of achieving a desired setpoint, but the squared form in (2c) is much easier to work with.

The quantities in 2 are defined for all time t since \mathbf{I}_{dq} and \mathbf{V}_{dq} are functions of t, but we are usually interested in optimizing the equilibrium values resulting from the dynamics in (1). Assuming that (1) is asymptotically stable (we show this in Section III-B), we denote the equilibrium of current and voltage as $\overline{\mathbf{I}}_{\mathrm{dq}}$ and $\overline{\mathbf{V}}_{\mathrm{dq}}$, respectively. Substituting these into (2), we get the equilibrium values of \overline{P} , \overline{Q} and $\overline{V}_{\mathrm{dq}}^2$. We

are interested in two related questions: 1) finding the optimal values of \overline{P} , \overline{Q} and \overline{V}_{dq}^2 and 2) achieving these values by designing a feedback controller for the system in (1).

We first look at the question of optimizing the equilibrium values. Let $S_1, S_2 \in (\overline{P}, \overline{Q}, \overline{V}_{\mathrm{dq}}^2)$ denote some choice of two out of the three quantities. We are interested in solving the following problem:

minimize
$$f(S_1, S_2)$$

subject to $\bar{\mathbf{I}}_{dg} \in \mathcal{I}$, (3)

where $f:\mathbb{R}^2\to\mathbb{R}$ is some objective function. For example, suppose that we are interested in tracking some setpoints S_1^*, S_2^* as closely as possible. The objective would be $f(S_1, S_2) = \frac{1}{2}(S_1 - S_1^*)^2 + \gamma \frac{1}{2}(S_2 - S_2^*)^2$ with γ being some tradeoff parameter.

It is not immediately clear whether the problem (3) is easy to solve. Even if f is a convex function, the quadratic forms in (2) make the overall problem not convex in $\bar{\mathbf{I}}_{dq}$.

C. Feasible Operating Regions

We can rewrite (3) as an optimization over S_1 and S_2 :

minimize
$$f(S_1, S_2)$$

subject to $(S_1, S_2) \in \mathcal{S}$ (4)

where S is the set of all feasible points achieved by currents $\overline{\mathbf{I}}_{\mathrm{dq}} \in \mathcal{I}$. In the next section, we show that S is convex, and consequently, (4) is a convex optimization problem if f is convex. Using the tracking example again, (4) with $f(S_1, S_2) = \frac{1}{2}(S_1 - S_1^*)^2 + \gamma \frac{1}{2}(S_2 - S_2^*)^2$ can be solved efficiently, allowing us to achieve perfect tracking if possible, and the closest setpoints if not.

III. GEOMETRY OF THE FEASIBLE REGION

In this section, we study the geometry of the feasible set S. The main result is given by Theorem 1.

Theorem 1. Let (S_1, S_2) be a pair of points formed by choosing any two of the three quantities $\overline{P}, \overline{Q}, \overline{V}_{dq}^2$. Let $S \in \mathbb{R}^2$ be the set of all achievable points (S_1, S_2) by $\overline{\mathbf{I}}_{dq} \in \mathcal{I}$. Then S is convex.

The proof of this theorem is given in the next section. Figure 2 plots what the regions look like for the combinations of $(P,Q),(P,V_{\rm dq}^2)$, and $(Q,V_{\rm dq}^2)$. The exact regions depend on the network parameters (R and L values as well as the grid voltage). We note that the shape of these regions depends on the fact that $\bf A$ is skew symmetric and has equal diagonal elements. Without this structure, these regions would not be convex.

A. Proof of Theorem 1

The first step in the proof is to write the quantities in (2) just as a function of the current. At equilibrium, the steady state voltage is

$$\overline{\mathbf{V}}_{\mathrm{dq}} = \mathbf{E}_{\mathrm{dq}} - L\mathbf{A}\overline{\mathbf{I}}_{\mathrm{dq}}.$$

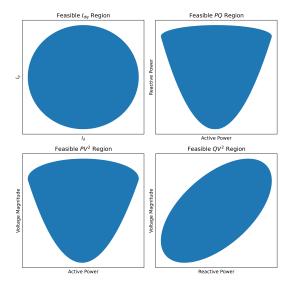


Fig. 2. The set of feasible inverter currents (\mathcal{I}) (top left) always forms a circle of radius I_{\max} due to the magnitude constraint on \mathbf{I}_{dq} . The shapes of feasible $(P,Q),(P,V_{\mathrm{dq}}^2)$, and (Q,V_{dq}^2) regions depend on specific network parameters, namely line impedance and grid-side voltage. Examples of these regions are shown in the top right, bottom left, and bottom right, respectively, for different network parameters.

Substituting this into (2), we have

$$\overline{P} = \frac{3}{2} \overline{\mathbf{I}}_{dq}^{T} (\mathbf{E}_{dq} - L\mathbf{A}\overline{\mathbf{I}}_{dq})$$
 (5a)

$$\overline{Q} = \frac{3}{2} \overline{\mathbf{I}}_{dq}^{T} \mathbf{J} (\mathbf{E}_{dq} - L \mathbf{A} \overline{\mathbf{I}}_{dq})$$
 (5b)

$$V_{\rm dq}^2 = (\mathbf{E}_{\rm dq} - L\mathbf{A}\bar{\mathbf{I}}_{\rm dq})^T (\mathbf{E}_{\rm dq} - L\mathbf{A}\bar{\mathbf{I}}_{\rm dq}). \tag{5c}$$

Using the fact that for any square matrix \mathbf{M} and vector \mathbf{z} , $\mathbf{z}^T \mathbf{M} \mathbf{z} = \mathbf{z}^T \frac{\mathbf{M} + \mathbf{M}^T}{2} \mathbf{z}$ and $\frac{\mathbf{A} + \mathbf{A}^T}{2} = \begin{bmatrix} -\frac{R}{L} & 0 \\ 0 & -\frac{R}{L} \end{bmatrix} = -\frac{R}{L} \mathbf{I}_2$ (where \mathbf{I}_2 is the 2 by 2 identity matrix), (5) becomes

$$\overline{P} = \frac{3}{2}R||\overline{\mathbf{I}}_{dq}||_2^2 + \frac{3}{2}\mathbf{E}_{dq}^T\overline{\mathbf{I}}_{dq}$$
(6a)

$$\overline{Q} = \frac{3}{2}\omega L ||\overline{\mathbf{I}}_{dq}||_2^2 + \frac{3}{2}\mathbf{E}_{dq}^T \mathbf{J}\overline{\mathbf{I}}_{dq}$$
(6b)

$$V_{\rm dq}^2 = (R^2 + \omega^2 L^2) ||\bar{\mathbf{I}}_{\rm dq}^2||_2^2 + 2\mathbf{E}_{\rm dq}^T \mathbf{A} \bar{\mathbf{I}}_{\rm dq} + ||\mathbf{E}_{\rm dq}||_2^2.$$
 (6c)

Because of the particular form of these equations, Theorem 1 follows directly from the following Lemma.

Lemma 1. Given linearly independent $\mathbf{a}, \mathbf{b} \in \mathbb{R}^2$ and $\alpha, \beta \in \mathbb{R}_+$, the set $C = \{(\alpha \mathbf{x}^T \mathbf{x} + \mathbf{a}^T \mathbf{x}, \beta \mathbf{x}^T \mathbf{x} + \mathbf{b}^T \mathbf{x}) \mid \mathbf{x}^T \mathbf{x} \leq 1\}$ is convex.

To apply Lemma 1 to our problem, first note that the constant term, $||\mathbf{E}_{\mathrm{dq}}||_2^2$, can be ignored. We also note that a, b will always be linearly independent: the linear terms in (6a) and (6b), proportional to \mathbf{E}_{dq} and $\mathbf{J}^T\mathbf{E}_{\mathrm{dq}}$, respectively, are orthogonal. The linear term in (6c) is proportional to $\mathbf{A}^T\mathbf{E}_{\mathrm{dq}}$ which is a linear combination of the linear terms in (6a) and (6b). Thus, each of the three vectors is linearly independent with respect to any one of the other two vectors and the Lemma holds for these equations.

Proof. To see this, we first rewrite C as

$$\left\{ \begin{bmatrix} \alpha ||\mathbf{x}||_2^2 \\ \beta ||\mathbf{x}||_2^2 \end{bmatrix} + \begin{bmatrix} \mathbf{a}^T \\ \mathbf{b}^T \end{bmatrix} \mathbf{x} \mid ||\mathbf{x}||_2^2 \le 1 \right\}. \tag{7}$$

Then, we define a new set C' as the image of set C under an affine function given by:

$$C' = \left\{ \begin{bmatrix} \mathbf{a}^T \\ \mathbf{b}^T \end{bmatrix}^{-1} \mathbf{s} \mid \mathbf{s} \in C \right\} = \left\{ ||\mathbf{x}||_2^2 \mathbf{c} + \mathbf{x} \mid ||\mathbf{x}||_2^2 \le 1 \right\},$$
(8)

for vector $\mathbf{s} = (S_1, S_2) \in \mathcal{C}$ and arbitrary vector $\mathbf{c} \in \mathbb{R}^2$, determined by

$$\mathbf{c} = \begin{bmatrix} \mathbf{a}^T \\ \mathbf{b}^T \end{bmatrix}^{-1} \begin{bmatrix} \alpha \\ \beta \end{bmatrix}.$$

The linear independence of a, b ensures the matrix inverse exists. Since convexity is preserved under affine transformations [19], it suffices to show the convexity of C'.

We now apply the definition of convexity to prove \mathcal{C}' is convex. We will show for any $\lambda \in [0,1]$ and any $\mathbf{x_1}, \mathbf{x_2}$ with $||\mathbf{x_1}||_2^2 \leq 1, ||\mathbf{x_2}||_2^2 \leq 1, \ \exists \mathbf{y} \in \mathcal{C}'$ such that

$$\|\mathbf{y}\|_{2}^{2} \mathbf{c} + \mathbf{y} = (\lambda \|\mathbf{x}_{1}\|_{2}^{2} + (1-\lambda)\|\mathbf{x}_{2}\|_{2}^{2}) \mathbf{c} + \lambda \mathbf{x}_{1} + (1-\lambda)\mathbf{x}_{2},$$

and $\|\mathbf{y}\|_{2}^{2} \le 1$. (9)

Note that because $\lambda = 0$ and $\lambda = 1$ result in the trivial cases of $\mathbf{y} = \mathbf{x}_1$ and $\mathbf{y} = \mathbf{x}_2$, we assume that $0 < \lambda < 1$. We recognize from (9) that \mathbf{y} must be of the form:

$$\mathbf{y} = \mu \mathbf{c} + \mathbf{z}$$
, where (10)

$$\mu = \lambda \|\mathbf{x_1}\|_2^2 + (1 - \lambda)\|\mathbf{x_2}\|_2^2 - \|\mathbf{y}\|_2^2.$$
 (11)

and $\mathbf{z} = \lambda \mathbf{x_1} + (1 - \lambda) \mathbf{x_2}$

The existence of \mathbf{y} depends on finding μ that satisfies (11) and results in $||\mathbf{y}||_2^2 \leq 1$. The following steps prove mathematically what is shown visually in Figure 3: at least one solution for μ to (11) will always lie within the bounds on μ determined by $||\mathbf{y}||_2^2 \leq 1$.

First, we define $f_1(\mu)$ by substituting (10) into (11) and $f_2(\mu)$ by substituting (10) into $||\mathbf{y}||_2^2 \le 1$:

$$f_1(\mu) = \|\mathbf{c}\|_2^2 \mu^2 + (2\mathbf{c}^T \mathbf{z} + 1)\mu + (\|\mathbf{z}\|_2^2 - \zeta) = 0,$$
 (12)

$$f_2(\mu) = \|\mathbf{c}\|_2^2 \mu^2 + (2\mathbf{c}^T \mathbf{z})\mu + (\|\mathbf{z}\|_2^2 - 1) \le 0,$$
 (13)

where $\zeta = \lambda \|\mathbf{x}_1\|_2^2 + (1-\lambda)\|\mathbf{x}_2\|_2^2 \le 1$, and $\|\mathbf{z}\|_2^2 \le \zeta$ by the triangle inequality for norms. Note that both parabolas open upwards ($\|\mathbf{c}\|_2^2 \ge 0$), and the constant terms of (12) and (13) are both negative so each equation will have one positive and one negative root. Denoting the roots of $f_1(\mu)$ as μ^- and μ^+ and the roots of $f_2(\mu)$ as μ and $\overline{\mu}$, we need at least one of μ^- or μ^+ to fall within the interval $[\mu, \overline{\mu}]$ as shown in Figure 3.

We show $\mu^+ \in [\underline{\mu}, \overline{\mu}]$ always holds by comparing the zeros and derivatives of (12) and (13). Observe first that $f_1(0) = ||\mathbf{z}||_2^2 - \zeta$ and $f_2(0) = ||\mathbf{z}||_2^2 - 1$, meaning $f_2(0) \leq f_1(0) \leq 0$ because $\zeta \leq 1$. Next, for $\mu > 0$, $\frac{\mathrm{d}f_1(\mu)}{\mathrm{d}\mu} = 2\|\mathbf{c}\|_2^2\mu + 2\mathbf{c}^T\mathbf{z} + 1$ will always be greater than $\frac{\mathrm{d}f_2(\mu)}{\mathrm{d}\mu} = 2\|\mathbf{c}\|_2^2\mu + 2\mathbf{c}^T\mathbf{z}$. Geometrically, this means for $\mu \in \mathbb{R}_+$, the quadratic $f_1(\mu)$ always lies above $f_2(\mu)$ with greater slope, so it will reach $f_1(\mu^+) = 0$ for a lower (but still positive) value of μ than $f_2(\overline{\mu})$. Therefore,

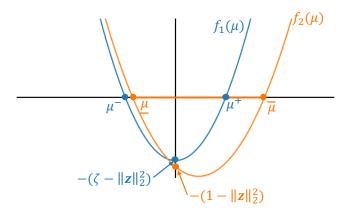


Fig. 3. Graphical representation of the quadratic equation $f_1(\mu)$ with its roots and quadratic inequality $f_2(\mu) \leq 0$ that corresponds to the interval $\mu \in [\underline{\mu}, \overline{\mu}]$. Convexity of set $\mathcal C$ depends on at least one of μ^-, μ^+ falling within this interval.

 $\underline{\mu} \le \mu^+ \le \overline{\mu}$ will always hold, proving y from (9) exists and set \mathcal{C} is convex.

Theorem 1 shows that for any two combinations of P, Q, V_{dq}^2 , the feasible region is convex. But it does not immediately provide a way to solve (4), since it does not directly give an algebraic description of the set. However, as the next theorem shows, we can describe the set using linear matrix inequalities.

Lemma 2. Let **W** be a 3 by 3 matrix and define \hat{C} as

$$\hat{C} = \{ (\text{Tr}(\mathbf{M}_1 \mathbf{W}), \text{Tr}(\mathbf{M}_2 \mathbf{W}) | W_{11} + W_{22} \le 1, W_{33} = 1, \mathbf{W} \succeq 0 \},$$

where

$$\mathbf{M}_{1} = \begin{bmatrix} \mathbf{I}_{2} & \frac{1}{2}\mathbf{a} \\ \frac{1}{2}\mathbf{a}^{T} & \zeta_{1} \end{bmatrix} \text{ and } \mathbf{M}_{2} = \begin{bmatrix} \mathbf{I}_{2} & \frac{1}{2}\mathbf{b} \\ \frac{1}{2}\mathbf{b}^{T} & \zeta_{2} \end{bmatrix}, \tag{14}$$

where ζ is an arbitrary constant. Then with \mathcal{C} defined as in Lemma 1, we have $\mathcal{C} = \hat{\mathcal{C}}$.

Proof. We first show that $\operatorname{Conv}(\mathcal{C}) = \hat{\mathcal{C}}$, where $\operatorname{Conv}(\mathcal{C})$ is the convex hull of \mathcal{C} . Observe we can write the equation in (6) in the form of $\begin{bmatrix} \mathbf{x} \\ 1 \end{bmatrix}^T \mathbf{M} \begin{bmatrix} \mathbf{x} \\ 1 \end{bmatrix}$ for some matrix M. Then note that the feasible set of \mathbf{W} is the convex hull of the feasible set for \mathbf{x} :

$$\{W_{11} + W_{22} \le 1, W_{33} = 1, \mathbf{W} \succeq 0\}$$

= $\operatorname{Conv}\left(\left\{\begin{bmatrix} \mathbf{x} \\ 1 \end{bmatrix}, ||x||_2^2 \le 1\right\}\right).$

Then by the linearity of the trace operator, $\operatorname{Conv}(\mathcal{C}) = \hat{\mathcal{C}}$. By Lemma 1, \mathcal{C} is convex, so we have $\mathcal{C} = \operatorname{Conv}(\mathcal{C}) = \hat{\mathcal{C}}$.

Lemma 2 shows that we can find optimal steady-state current values by solving

$$\min f(\operatorname{Tr}(\mathbf{M}_1\mathbf{W}_1) \operatorname{Tr}(\mathbf{M}_2\mathbf{W})) \tag{15a}$$

s.t.
$$W_{11} + W_{22} \le I_{\text{max}}^2$$
 (15b)

$$W_{33} = 1$$
 (15c)

$$\mathbf{W} \succeq 0, \tag{15d}$$

where $\mathbf{M}_1, \mathbf{M}_2$ can be chosen to be $\begin{bmatrix} \frac{3}{2}R\mathbf{I}_2 & \frac{3}{4}\mathbf{E}_{\mathrm{dq}} \\ \frac{3}{4}\mathbf{E}_{\mathrm{dq}}^T & 0 \end{bmatrix}$ for P, $\begin{bmatrix} \frac{3}{2}\omega L\mathbf{I}_2 & \frac{3}{4}\mathbf{J}^T\mathbf{E}_{\mathrm{dq}} \\ \frac{3}{4}\mathbf{E}_{\mathrm{dq}}^T\mathbf{J} & 0 \end{bmatrix}$ for Q and $\begin{bmatrix} (R^2 + \omega^2 L^2)\mathbf{I}_2 & \mathbf{A}^T\mathbf{E}_{\mathrm{dq}} \\ \mathbf{E}_{\mathrm{dq}}^T\mathbf{A} & ||\mathbf{E}_{\mathrm{dq}}||_2^2 \end{bmatrix}$ for $\mathbf{V}_{\mathrm{dg}}^2$.

The previous results in this paper state that, given feasible \mathbf{W} to (15), we can find a feasible current $\overline{\mathbf{I}}_{dq}$ that achieves the same objective value. However, they do not directly show that the optimal solution to (15) is always rank 1. We can easily solve a quadratic equation (cf. proof of Lemma 1) to find the corresponding $\overline{\mathbf{I}}_{dq}$, but an interesting observation from numerical simulations is that the solution to (15) is always rank 1 (possibly with a small regularization term on the nuclear norm of \mathbf{W}). An important part of our future work is to rigorously prove this observation.

B. Inverter Control

Given the steady-state values \overline{I}_{dq} for (1), we need to find a voltage controller such that the current will reach this equilibrium. In other words, we need to track the corresponding equilibrium voltage to \overline{I}_{dq} :

$$\overline{\mathbf{V}}_{\mathrm{dq}} = \mathbf{E}_{\mathrm{dq}} - L\mathbf{A}\overline{\mathbf{I}}_{\mathrm{dq}}.$$

We implement linear feedback control on $V_{\rm dq}$ to achieve $\overline{V}_{\rm dq}$:

$$\dot{\mathbf{V}}_{\mathrm{dq}} = -k_v(\mathbf{V}_{\mathrm{dq}} - \overline{\mathbf{V}}_{\mathrm{dq}}), \tag{16}$$

where k_v is a positive proportional gain constant. It is easy to show that the closed-loop system is always stable (e.g., by computing the eigenvalues), and the trajectories remains within \mathcal{I} with a correctly chosen k_v [15].

We point out an important difference between our controller and some existing droop-based controllers, especially in the context of grid-forming control. The control loops in grid-forming inverters are designed to operate without needing to know the parameters of the system (e.g., the R, L and grid voltage) [20], [21]. In the methods present in this paper, we need these values to compute the feasible region. Of course, existing control loops cannot enforce safety or optimality. We believe the geometry of teh problem is "nice" enough and our methods can be adapted to the case where the parameters are not known, and we address this in a follow-up work.

IV. CASE STUDY

To numerically test this controller, we simulate the inverter network's response tracking a variety of feasible and infeasible setpoints. We compare the optimal controller's (OC) performance in tracking (P^*,Q^*) and $(P^*,V_{\mathrm{dq}}^{2*})$ setpoints to standard droop controllers adapted from [22]. The droop controllers operate by first filtering the inverter's active and

TABLE I SIMULATION PARAMETERS

| Parameter | Value | Droop Param. | Value | |
|-------------------------|------------------------|---|-------------------------------------|--|
| R | 0.8 Ω | m_p | $2.6 \times 10^{-3} \text{ rad/sW}$ | |
| L | 1.5 mH | m_q | 5.0×10^{-3} V/VAr | |
| E | 120 V | m_{v^2} | 5.0 | |
| ω_{nom} | $2\pi60 \text{ rad/s}$ | $egin{array}{c} m_{v^2} \ \omega_c \end{array}$ | $2\pi60 \text{ rad/s}$ | |
| $I_{\rm dg,nom}$ | 3.33 A | | | |
| $V_{\rm dq,nom}$ | 120 V | OC Param. | Value | |
| $S_{\mathrm{inv,nom}}$ | 1200 W | k_v | 10 | |

TABLE II $P^*, Q^*, V^{2*} \mbox{ SETPOINTS USED IN SIMULATIONS}$

| | | $P^*(W)$ | $Q^*(VAr)$ | $V_{ m dq}^{2*}({ m V}^2)$ |
|-----------------|------------------|----------|------------|----------------------------|
| \overline{PQ} | Pre-Disturbance | 800 | 0 | _ |
| Tracking | Post-Disturbance | 1100 | 0 | _ |
| PV^2 | Pre-Disturbance | 200 | _ | 120^{2} |
| Tracking | Post-Disturbance | 850 | _ | 120^{2} |
| QV^2 | Pre-Disturbance | _ | 0 | 120^{2} |
| Tracking | Post-Disturbance | _ | -500 | 120^{2} |

reactive power (P,Q) through a low-pass filter with cut-off frequency ω_c to measure \tilde{P} and \tilde{Q} . These filtered values have the following dynamics $\dot{\tilde{P}} = \omega_c (P - \tilde{P}) \ \dot{\tilde{Q}} = \omega_c (Q - \tilde{Q})$.

Then, voltage magnitude droop dynamics and frequency droop are implemented as $\dot{V}_{\rm dq}=m_q\omega_c(\tilde{Q}-Q)$ and $\Delta\omega_i=-m_p(\tilde{P}-P^*)$, where $\Delta\omega_i$ is the deviation of inverter frequency from grid frequency and m_p and m_q are proportional gain parameters. These follow from $\Delta V_{\rm dq}=-m_q(\tilde{Q}-Q^*)$, where $\Delta V_{\rm dq}$ is the deviation in voltage magnitude from a desired $V_{\rm dq,nom}$ value.

The PV^2 droop controller has the same low-pass PQ filter and power-frequency dynamics as the PQ droop controller, but it replaces the reactive power-voltage dynamics with linear feedback on $V_{\rm dq}^2$ as $\dot{V}_{\rm dq}^2 = -m_{v^2}(V_{\rm dq}^2 - V_{\rm dq}^{2*})$. Parameters for the PQ and PV^2 droop controllers are listed in Table I (adapted from [22]).

To implement the optimal controller, we select the appropriate matrices \mathbf{M}_1 , \mathbf{M}_2 for the variables we seek to track and solve (15) for the optimal \mathbf{W} and corresponding optimal equilibrium current $\bar{\mathbf{I}}_{dq}$. We use the CLARABEL solver in CVXPY [23]. We then implement linear feedback control on \mathbf{V}_{dq} as described in (16) with value of k_v found in Table I.

Simulations for both droop and optimal controllers are conducted using the SciPy odeint solver with a sampling time of $\Delta t = 100 \mu s$ and simulation period of $t_{\rm end} = 1s$. Reference setpoints used in the simulations are provided in Table II where the disturbance is modeled as a change in setpoints at time t_0 from pre- to post-disturbance values.

A. P-Q Tracking

Our first example compares the responses of the OC and droop controllers tracking a 300W increase in the active power setpoint at t_0 . As seen in Figure 4, the trajectory of the droop controller (blue) is unsafe; it temporarily leaves the feasible operating region shown in gray despite reaching a safe equilibrium. The optimal controller (orange) keeps the inverter within its current limit throughout the simulation.

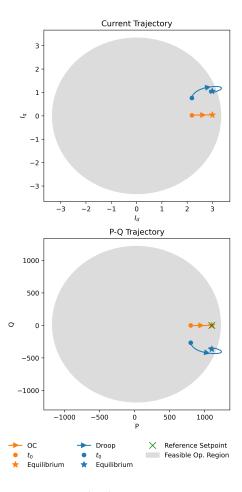


Fig. 4. Tracking a feasible P^*,Q^* setpoint using droop control (blue) and the optimal controller (orange). Trajectories are shown in the \mathbf{I}_{dq} region (top) and the corresponding (P,Q) region (bottom) with safe operating regions shaded in gray. The optimal controller ensures the inverter remains within its operating limits throughout the simulation and can track constant P^* and Q^* setpoints with zero steady-state error - two advantages over droop control.

It is also of note that the optimal controller perfectly tracks (feasible) P^* and Q^* setpoints: the equilibrium reached in Figure 4 matches the reference setpoint. In contrast, the droop controller has non-zero steady-state error tracking a constant Q^* reference signal which is a limitation of proportional controllers for QV droop.

B. P- $V_{\rm dq}^2$ Tracking

To demonstrate how the OC and droop controllers handle infeasible setpoints (reference values that lie outside the safe operating region of the inverter), we simulate the responses to a 650W increase in active power setpoint with a constant voltage magnitude setpoint of 120V. In this case, when the optimal controller solves (15), the safety constraints become binding and the optimization finds the current associated with the closest feasible $(\overline{P}, \overline{V}_{\rm dq}^2)$ setpoint to $P^* = 850$, $V_{\rm dq}^{2*} = 120^2$. Thus, as shown in Figure 5, the optimal controller settles at the boundary of the inverter operating region. The droop controller, however, has no current limiting in place, so it tracks the infeasible setpoint as given causing it to exceed device limits.

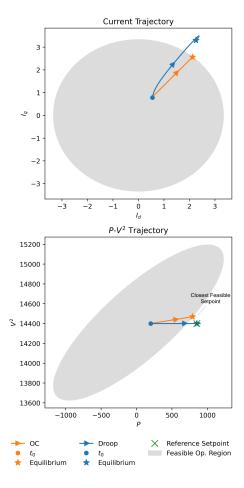


Fig. 5. Tracking an infeasible P^*, V^{2*} setpoint using droop control (blue) and the optimal controller (orange). Trajectories are shown in the \mathbf{I}_{dq} region (top) and the corresponding (P,V^2) region (bottom) with safe operating regions shaded in gray. The optimal controller finds and tracks the closest safe operating point (on the boundary of the inverter's operating region) instead of the original infeasible setpoint, while the droop controller ignores device limits and settles at an unsafe equilibrium current.

C. Q- $V_{\rm dg}^2$ Tracking

Finally, we note that our approach can track a change in Q^*, V^{2*} setpoints. The optimal controller follows the same procedure as for (P,Q) and (P,V^{2*}) tracking, resulting in safe transient and steady-state currents. This flexibility to provide (Q^*,V^{2*}) tracking is another advantage of the optimal controller over droop control. Droop controllers typically depend on the relationship between voltage and reactive power to implement Q-droop so they cannot easily track independent setpoints in Q and V.

V. CONCLUSION

In this paper, we studied the geometry of the feasible output region of a current-limited inverter. We showed that this region is convex and can be described using linear matrix inequalities. We demonstrated that how to use this fact to design safe controllers such that transient trajectories always remain within the current magnitude limit. Some future directions include showing the semidefinite program always returns a rank one solution, and how the controllers can be designed when the detailed parameters are not known.

REFERENCES

- P. Kundur, N. J. Balu, and M. G. Lauby, Power system stability and control. McGraw-hill New York, 1994, vol. 7.
- [2] B. Fan, T. Liu, F. Zhao, H. Wu, and X. Wang, "A review of current-limiting control of grid-forming inverters under symmetrical disturbances," *IEEE Open Journal of Power Electronics*, vol. 3, pp. 955–969, 2022.
- [3] N. Baeckeland, D. Chatterjee, M. Lu, B. Johnson, and G.-S. Seo, "Overcurrent limiting in grid-forming inverters: A comprehensive review and discussion," *IEEE Transactions on Power Electronics*, 2024.
- [4] A. Elnaggar, J. L. Rueda, and I. Erlich, "Comparison of short-circuit current contribution of doubly-fed induction generator based wind turbines and synchronous generator," in 2013 IEEE Grenoble Conference. IEEE, 2013, pp. 1–6.
- [5] A. Hooshyar and R. Iravani, "Microgrid protection," *Proceedings of the IEEE*, vol. 105, no. 7, pp. 1332–1353, 2017.
- [6] I. S. Association et al., "Ieee standard for interconnection and interoperability of inverter-based resources (ibrs) interconnecting with associated transmission electric power systems," *IEEE Std*, pp. 2800–2022, 2022.
- [7] A. D. Paquette and D. M. Divan, "Virtual impedance current limiting for inverters in microgrids with synchronous generators," *IEEE Transactions* on *Industry Applications*, vol. 51, no. 2, pp. 1630–1638, 2014.
- [8] Q.-C. Zhong and G. C. Konstantopoulos, "Current-limiting droop control of grid-connected inverters," *IEEE Transactions on Industrial Electron*ics, vol. 64, no. 7, pp. 5963–5973, 2016.
- [9] D. Pattabiraman, R. H. Lasseter, and T. M. Jahns, "Comparison of grid following and grid forming control for a high inverter penetration power system," in 2018 IEEE Power & Energy Society General Meeting (PESGM). IEEE, 2018, pp. 1–5.
- [10] P. Christensen, G. K. Andersen, M. Seidel, S. Bolik, S. Engelken, T. Knueppel, A. Krontiris, K. Wuerflinger, T. Bülo, J. Jahn et al., "High penetration of power electronic interfaced power sources and the potential contribution of grid forming converters," European Network of Transmission System Operators for Electricity, 2020.
- [11] Y. Li, Y. Gu, and T. C. Green, "Revisiting grid-forming and grid-following inverters: A duality theory," *IEEE Transactions on Power Systems*, vol. 37, no. 6, pp. 4541–4554, 2022.
- [12] P. Hart and B. Lesieutre, "Energy function for a grid-tied, droop-controlled inverter," in 2014 North American Power Symposium (NAPS). IEEE, 2014, pp. 1–6.
- [13] T. Qoria, F. Gruson, F. Colas, X. Kestelyn, and X. Guillaud, "Current limiting algorithms and transient stability analysis of grid-forming vscs," *Electric Power Systems Research*, vol. 189, p. 106726, 2020.
- [14] T. Joswig-Jones and B. Zhang, "Optimal control of grid-interfacing inverters with current magnitude limits," in 2024 IEEE 63rd Conference on Decision and Control (CDC). IEEE, 2024, pp. 4623–4628.
- [15] —, "Safe control of grid-interfacing inverters with current magnitude limits," in *Hawaii International Conference on System Sciences (HICSS)*, 2025.
- [16] A. Yazdani and R. Iravani, Voltage-Sourced Converters in Power Systems: Modeling, Control, and Applications, ser. IEEE Press. Wiley, 2010. [Online]. Available: https://books.google.com/books?id=_x_4Cu-BKwkC
- [17] F. L. Luo and H. Ye, Advanced DC/AC inverters: applications in renewable energy. Crc Press, 2017.
- [18] N. Bottrell and T. C. Green, "Comparison of current-limiting strategies during fault ride-through of inverters to prevent latch-up and wind-up," *IEEE Transactions on Power Electronics*, vol. 29, no. 7, pp. 3786–3797, 2013.
- [19] S. Boyd and L. Vandenberghe, Convex Optimization. Cambridge University Press, 2004.
- [20] Y. Gu and T. C. Green, "Power system stability with a high penetration of inverter-based resources," *Proceedings of the IEEE*, vol. 111, no. 7, pp. 832–853, 2022.
- [21] L. Huang, H. Xin, Z. Wang, L. Zhang, K. Wu, and J. Hu, "Transient stability analysis and control design of droop-controlled voltage source converters considering current limitation," *IEEE Transactions on Smart Grid*, vol. 10, no. 1, pp. 578–591, 2017.
- [22] M. Lu, V. Purba, S. Dhople, and B. Johnson, "Comparison of droop control and virtual oscillator control realized by andronov-hopf dynamics," in *IECON 2020 The 46th Annual Conference of the IEEE Industrial Electronics Society*, 2020, pp. 4051–4056.
- [23] S. Diamond and S. Boyd, "CVXPY: A Python-embedded modeling language for convex optimization," *Journal of Machine Learning Research*, vol. 17, no. 83, pp. 1–5, 2016.